An Optimal Wind Farm Operation Strategy for the Provision of Frequency Containment Reserve Incorporating Active Wake Control

Nezmin Kayedpour, *Student Member, IEEE,* Jeroen D. M. De Kooning, *Senior Member, IEEE,* Arash E. Samani, *Student Member, IEEE,* Farjam Kayedpour, Lieven Vandevelde, *Senior Member, IEEE,* and Guillaume Crevecoeur

***Abstract*—This study proposes a novel operation strategy for wind farms' optimal Frequency Containment Reserve (FCR) provision that simultaneously distributes FCR and optimally controls wake formation. The power reserve allocation is dynamically decided at the wind farm supervisory control level, considering the intermittent wind power and direction, grid frequency stochasticity, and the aerodynamic complexity of the wake. A two-stage stochastic programming approach supports decision-making for an optimal contribution to day-ahead energy/FCR markets considering sub-hourly wind power and grid frequency uncertainty. Moreover, a novel method is used to reduce the computational complexity by employing a data-driven surrogate model of wake formation in the optimizer. This surrogate model consists of a neural network trained on the Gauss-Curl-Hybrid wake model in FLORIS. This deep learning approach allows fast estimation of the wake control parameters, i.e., the optimal yaw angles and axial induction factors. Then, a coevolutionary-based multi-objective particle swarm optimization searches for the optimal deloading of the WTs and maximizes the total power production and kinetic energy while minimizing wake. The performance of the proposed algorithm is evaluated on the C-Power wind farm layout in the North Sea. Simulation results demonstrate its effectiveness in improving the wind farm's overall performance for different operational conditions.**

***Index Terms*—Wind energy, Deep learning, Axial induction factor, Optimization, Flexible operation, Day-ahead market.**

I. Introduction

THE European Union (EU) is dedicated to becoming the global leader in decarbonizing the power system. Wind power is essential in reaching the EU carbon-neutral target by 2050 [1]. However, effective integration of wind energy into the power system can raise concerns about grid stability and reliability due to the intrinsic stochastic nature of wind [2]. The primary reason for the blackout events on 9 August 2019 in the UK was the sudden decline in frequency beyond the regulation capability of system inertia [3]. As a result, there is a significant demand from Transmission System Operators (TSO) for wind energy sources to play an active role in balancing the grid through market participation and provision of ancillary services such as frequency control, which traditionally have been provided by conventional power plants. [4]. Nevertheless, how to effectively incorporate the ability to provide frequency support into the reliable and optimal operation of the system, accurately schedule the products of the frequency support, and efficiently distribute the power reserve within wind farms (WF) are still open challenges. This study aims to fill these gaps by proposing an optimal operation strategy considering all mentioned criteria.

Ancillary markets and other grid-balancing mechanisms have already been created for renewable energy sources in European countries. The participation of wind energy in reserve markets in Great Britain and Spain is analyzed in [5], and recommendations are made to support future development. [6] also explored the potential of wind power to enter the Swedish ancillary service markets, considering technical requirements and the potential financial impacts on a WF. The Belgian TSO has reported that offshore wind is expected to play a significant role in the Belgian power system in the near future [7]. Although wind energy has the capability to enter these markets, still some uncertainty regarding optimal contribution exists. A differentiated pricing scheme was used in [8] to propose a market mechanism design for inertia and primary frequency response, taking into account the energy market in which the system operator will participate in the joint market with a combined clearing process. While the methods described in [8], [9] have not considered the day-ahead scheduling, [9] leverages field-measured data to examine the frequency support capacity of a WF, and discusses the uncertainty of wind and frequency constraints. [10]–[12] discussed optimal bidding and scheduling strategies that optimize hour-ahead, intraday, and day-ahead operations while incorporating a shared frequency regulation reserve plan for wind, photovoltaic, and thermal power. However, these studies did not take into account the real-time dynamic interactions inside or between these energy sources. An advanced day-ahead bidding strategy for wind power producers is proposed in [13], considering the wind speed and system frequency uncertainties as stochastic inputs and a confidence level on the real-time reserve provision. In [14], optimal bidding strategies in the real-time electricity market are investigated for wind power

N. Kayedpour, J. D. M. De Kooning, A. E. Samani, L. Vandevelde, and G. Crevecoeur are with the Department of Electromechanical, Systems & Metal Engineering, Ghent University, Tech Lane Ghent Science Park - Campus Ardoyen, Technologiepark-Zwijnaarde 131, B-9052 Ghent, Belgium. N. Kayedpour, J. D. M. De Kooning, A. E. Samani, L. Vandevelde, and G. Crevecoeur are also with FlandersMake@UGent - Corelab MIRO. F. Kayedpour is with the Department of Industrial Management, Management, and Accounting Faculty, Allameh Tabatabai University, Tehran, Iran. (email: nezmin.kayedpour@ugent.be; jeroen.dekooning@ugent.be; ebnealisamani.arash@ugent.be; Kayedpour921@atu.ac.ir; lieven.vandevelde@ugent.be; and guillaume.crevecoeur@ugent.be).

generation using a bi-level stochastic optimization framework that maximizes profit by determining the optimal bidding quantity. However, the optimal distribution of the scheduled reserve among Wind Turbines (WT), taking into account the aerodynamic complexity of these sources, has not been considered by [13], [14].

Another critical element needed to facilitate wind integration into power systems is an advanced WF supervisory operation strategy that guarantees the optimal provision, allocation, and activation of power reserve in different operating conditions [15]. In a two-stage economic dispatch model, [16] and [17] incorporate wind power reserve but yet overlook the optimal reserve allocation in WFs. More recent studies suggested novel WF control strategies and approaches for enhancing the grid support, such as self-control via diode rectifier-based high voltage alternating current (HVAC) transmission system [18], error-based active disturbance rejection control for WT power regulation [19], deloading and curtailment methods [20], [21] that maintain an adequate power reserve for delivering an automatic and fast response to the TSO's demands. [22] introduced a scheme for model predictive control that harmonizes the functioning of offshore WTs and offshore DC collection grid capacitors to offer rapid inertia and primary frequency support. Nevertheless, the need for power reserve and frequency support amplifies the intricacies of WFs with linked aerodynamic systems, necessitating a more comprehensive examination. Studies have been carried out focusing on the aerodynamic coupling between WTs and their wake formation, which creates a wind energy deficit between the wind-leaving turbine (upstream WT) and the wind-arriving turbine (downstream WT). This phenomenon makes it difficult to determine exact energy extractions and justify the WFs' optimal contribution to frequency regulations [23].

Further studies have focused on determining the effectiveness of including inertial response and frequency control techniques, considering the apparent limitations of WFs compared to traditional power plants [24]–[26]. Applying these techniques often reduces wind energy production by a certain level of efficiency loss. [27] addressed harvesting maximum kinetic energy during the deloading control strategy using a game theory-based optimal control framework, which distributedly adjusts WTs' rotor speeds in a WF layout. Additional studies propose coordinated control approaches for WFs providing frequency control considering wake interactions inside the WF. In [28], a coordinated WF operation strategy is proposed that, instead of seeking to maximize the power generation of WTs individually, ensures the maximization of the rotational kinetic energy while maintaining the optimal WF's overall performance. A control algorithm is suggested in [29] to distribute the power reserve, aiming to minimize the wake effects and maximize the reserve capacity.

The mentioned studies either covered optimal bidding problems in the market or investigated WF optimal operation strategies without considering wake effects or market constraints. Although some research reveals optimization methods that can coordinate WTs and enable them to provide ancillary services optimally, time-efficient optimization approaches are lacking, considering the high complexities involved in wake models. In addition, the stochastic behavior of wind and grid frequency forms a perpetually varying environment, requiring online and dynamic strategies that can cope with high aerodynamic complexity and variability. This study aims to overcome the limitations of current approaches by developing an integrated algorithm that can effectively tackle the primary challenges associated with WF providing FCR, particularly when there are no ideal energy storage systems in place. The proposed algorithm will take an active approach to ensure that FCR provision is optimized at scheduling and activation levels. In [28], [30] and [31], the FCR provision was optimally distributed in a WF, taking into account wake interaction, using the Jensen wake model. However, the wake or wake parameters were not actively controlled as part of the optimization. The primary novelty of this article is to integrate active control of the wakes in the operation strategy, such that FCR distribution and wake control are optimized simultaneously. However, the integration of active wake control significantly increases the complexity of the optimization problem compared to [28], and [31]. This is resolved by the secondary novelty of this work, i.e., using a data-driven surrogate model of the wake formation in the optimizer, resulting in a computationally efficient optimal operation strategy. Moreover, the Gauss-Curl-Hybrid (GCH) wake model in the FLORIS wake simulator is used to generate the dataset instead of the simplified Jensen wake model. The contributions of this paper are three-fold:

1) A two-stage stochastic programming is proposed to optimize the contribution of a WF to the day-ahead energy and FCR markets while considering uncertainties related to wind speed and grid frequency. The approach involves using the Group Method of Data Handling (GMDH), a data-driven time-series prediction technique, to predict wind speed and grid frequency and calculate expected values for different scenarios.
2) An optimization framework incorporating active wake control is then suggested to dynamically distribute the pre-scheduled optimal power reserve among the WTs, restricted by optimal wake parameters (yaw angles and axial induction factors), which are being calculated and updated for varying operating conditions using a computationally efficient approach involving deep learning neural networks.
3) The integrated algorithm of optimal power reserve allocation is realized by proposing an adaptive WT local control system that can cope with the set points decided at the supervisory control level to adjust the power reserve margin based on the optimally estimated deloaded percentage.

The rest of this paper is organized as follows: § II propose the formulation of the WF operation strategy. § III introduces the stochastic programming framework for offering an optimal FCR provision based on wind and grid frequency prediction. § IV formulates the optimal operation strategy and allocation of power reserve by maximizing WF power production and total kinetic energy. § V provides an overview of the outcomes and results, while § VI summarises and concludes the paper.

II. Overview of the WF Operation Strategy

The proposed operational strategy is shown in Fig. 1. The presented concept relies on a two-step sequential framework. In the primary step, a two-stage stochastic programming problem estimates the WF's optimal contribution to the day-ahead energy and reserve markets, considering wind and grid frequency uncertainties. In the first stage, the model determines the optimal decision variables P_e^{sch} and P_r^{sch} based on the available information at the time of decision-making, such as the forecasted wind power output v and the grid frequency f_e employing the Group Method of Data Handling (GMDH), a data-driven time-series prediction technique. The decision variables include the amount of energy and reserve and the bids submitted to the market. In the second stage, the model takes into account the uncertainties associated with wind power generation and grid frequency, which can affect the actual outcomes of the first-stage decisions. The model considers a set of scenarios that represent different possible realizations of these uncertainties and evaluates the outcomes of the first-stage decisions under each scenario. The evaluation criteria include the expected profit, the risk of violating the reserve requirements, and the cost of deviation from the scheduled energy and reserve productions. The final decision is then made by considering the trade-off between the expected profit and the risk of violating the reserve requirements while ensuring the reliability of the WF operation.

Among different reserve products, this study only focuses on Frequency Containment Reserve (FCR), formerly known as the primary control, which helps maintain the stability of the power grid by providing a rapid response to sudden changes in frequency. The FCR provision is responsible for keeping the power system's frequency within an acceptable range, $\Delta f = 200\ mHz$ around the nominal frequency of $f_{ref} = 50\ Hz$, and reacting proportionally to the frequency changes. Automatic and manual Frequency Restoration Reserves (aFRR, mFRR) are other ancillary services, formerly known as secondary and tertiary control. Fig. 2 shows the provision and activation of these services. The aFRR and mFRR are reserve capacities that

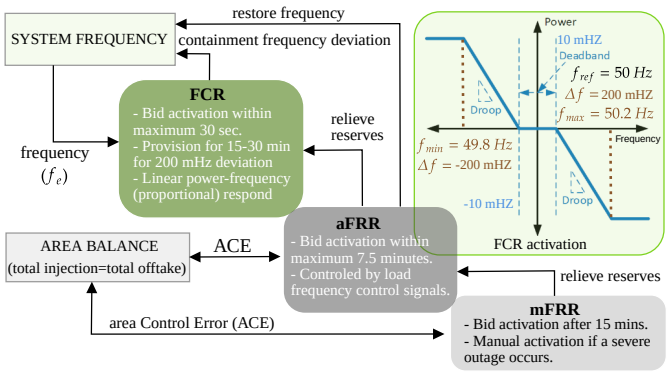

Figure 2: Provision of ancillary services.

play a crucial role in maintaining the stability of the power grid by restoring the system's frequency to its nominal value in the event of a disturbance. While the aFRR is automatically activated, the mFRR requires manual activation. This study considers FCR provision, which can introduce considerable challenges on WFs integrated control systems.

Once an ideal reserve P_r^{sch} has been determined in the day-ahead market, the subsequent stage involves the utilization of a second-layer optimization algorithm to actively allocate the scheduled power reserve among the WTs. This process involves the efficient computation of optimal wake parameters, such as optimal yaw angles y_i^{opt} and axial induction factors a_i^{opt}, through the use of an Adaptive Network-based Fuzzy Inference System (ANFIS) framework. The ANFIS structure is capable of learning and replicating the wake behavior of the WF in various wind speeds, directions, and turbulence intensities (TI). The allocation of power reserve will be realized by sending WTs' setpoints, i.e., deloaded rotational speed ω_i^{dl}, and blade pitch offset θ_i^{offset}, and deloaded power $P_{w,i}^{dl}$, to the WTs' local control systems. After optimally deciding the WT's adjustable power reserve margin, the WT's look-up table will be adapted considering the estimated deloading percentage β. Eventually, activating FCR will be carried out by responding to frequency changes Δf through an FCR supplementary control loop.

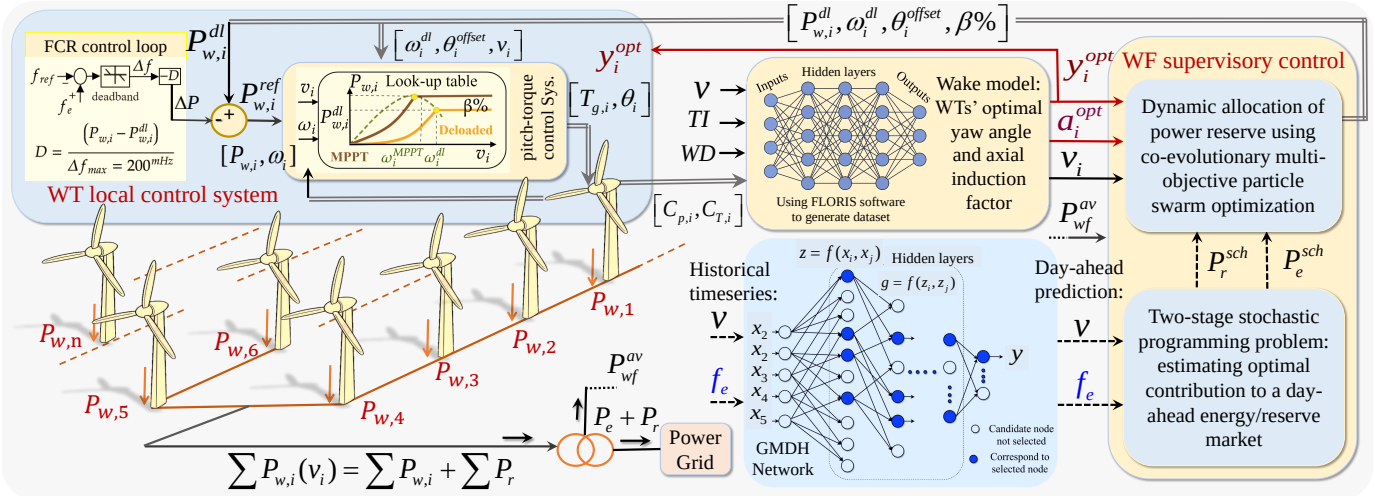

Figure 1: Proposed optimal operation strategy providing FCR.

III. Optimal FCR contribution

As mentioned, the proposed stochastic optimization framework aims to determine the strategic bidding for the scheduled reserve quantity in the day-ahead market at the market-clearing price and in a non-price-making position. Once the WF operator decides the bidding quantity, it will not be allowed to change its decision the next day against the signed corresponding transaction agreement. Therefore, a two-stage stochastic optimization process is formulated to support the decision-maker during the different stages considering the market restrictions. This strategy helps the operator make an optimal decision considering the day-ahead electricity and reserve transactions (first stage) and aids in optimizing tomorrow's real-time operations (second stage).

The GMDH method, which is a form of nonlinear regression, acts as a semi-supervised deep learning technique that can self-organize the predictive distribution of stochastic variables. By driving the optimal polynomial network structure, it can accurately reveal the approximated function and predict future values based on historical datasets. The GMDH time series prediction approach involves utilizing polynomial functions to express the general relationship between delayed inputs and output variables, known as the Volterra function series or the Kolmogorov-Gabor polynomial function expressed by:

$$y = a_0 + \sum_{i=1}^{m} a_i x_i + \sum_{i=1}^{m}\sum_{j=1}^{m} a_{ij} x_i x_j + \sum_{i=1}^{m}\sum_{i=1}^{m}\sum_{k=1}^{m} a_{ijk} x_i x_j x_k \tag{1}$$

In the given equation, the response variable is represented by 'y', while the vector of lagged time series to be regressed is represented by 'x'. The letter 'm' denotes the number of variables, and the weighting factors are represented by the coefficients a_0, a_i, a_{ij} and a_{ijk}. For this research, the quadratic K-G polynomial has been utilized and represented in the following form:

$$z = f(x_i, x_j) = b_0 + b_1 x_i + b_2 x_j + b_3 x_j x_i + b_4 x_i^2 + b_5 x_j^2 \tag{2}$$

The GMDH framework can be trained to learn the relationship between different lags using a function f. To accomplish this, a stochastic approximation algorithm is proposed, which is based on a multilayer network. Each layer of the network uses various component subsets of the polynomial function, with the output of the last layer being used as input for the next layer. The algorithm conducts regression polynomials of all possible combinations of two independent variables from a total of n inputs in the first layer. The minimum activation function is a second-order polynomial, but higher orders can be used to find the optimal complexity. A threshold is used to limit the number of solutions and to find the best structure based on an external criterion.

The grid frequency estimation is performed using the least-squares regression method over a period of five years of historical data from January 2015 to October 2019 with a 10-seconds time interval obtained from the website of the Belgian TSO Elia [32]. The wind speed dataset for the same period with a 15-minute sampling interval is obtained from a global weather API [33]. The prediction horizon is set to 24 hours with five delayed inputs. Fig. 3 illustrates the stochastic input parameters of the proposed problem. The quarter-hourly-based average grid frequency is estimated using the K-means algorithm that finds the average center of clusters located outside of the deadband zone. Also, around 400 wind speed scenarios are considered based on the historical data set. A scenario reduction suggested in [34] is used to reduce the computational complexity of the problem. The nonlinearity of the available WF power production considering wind speed, direct and turbulence intensity is estimated as follows:

$$P_{\mathrm{wf}} = \begin{cases} 0 \ \mathrm{MW} & , \quad 0 < \mathrm{v} < \mathrm{v}_{\mathrm{w}}^{\mathrm{ci}} \\ a\ v^3 + b\ v^2 + c\ v + d \ \mathrm{MW} & , \quad \mathrm{v}_{\mathrm{w}}^{\mathrm{ci}} \leqslant \mathrm{v} \leqslant \mathrm{v}_{\mathrm{w}}^{\mathrm{n}} \\ 149.73 \ \mathrm{MW} & , \quad \mathrm{v}_{\mathrm{w}}^{\mathrm{n}} \leqslant \mathrm{v} \leqslant \mathrm{v}_{\mathrm{w}}^{\mathrm{cu}} \end{cases} \tag{3}$$

where $v_{\mathrm{w}}^{\mathrm{ci}}$, $v_{\mathrm{w}}^{\mathrm{cu}}$ and $v_{\mathrm{w}}^{\mathrm{n}}$ are respectively the cut-in, cut-out and nominal wind speeds in m/s. P_{wf} is the WF total electrical power in MW. a, b, c, and d are the parameters of a cubic polynomial fitted to the data. A deep learning time-series forecasting method is conducted using the GMDH to compute each scenario's expected value [35].

The bidding decision variables of electricity production P_e^{sch} and reserve P_r^{sch} are first-stage decision variables that should be scheduled a day before the activation. Once the WF owner decides on the FCR contribution, it will not be allowed to change its decision the next day. Therefore, the second stage should consider the possible scenarios and their expected values. The optimization framework and the constraints are:

$$\max \begin{bmatrix} \left(P_e^{\mathrm{sch}} \cdot \lambda_e^{\mathrm{sch}} + P_r^{\mathrm{sch}} \cdot \lambda_r^{\mathrm{sch}}\right) \cdot \Delta T + \\ \mathrm{E}_s \left(\left(\Delta P_e(s) \cdot \lambda_{\Delta e} + \Delta P_r(s) \cdot \lambda_{\Delta r}\right) \cdot \Delta T \right) \end{bmatrix} \tag{4}$$

$$P_{\mathrm{wf}} = P_r(s) + P_e(s) \tag{5}$$

$$\Delta P_e = \left| P_e(s) - P_e^{\mathrm{sch}} \right| \ ; \ \Delta P_r = \left| P_r(s) - P_r^{\mathrm{sch}} \right| \tag{6}$$

$$\Delta P_e(s) \cdot \lambda_{\Delta e} = \Delta P_e^{+}(s) \cdot \lambda_{\Delta e}^{+} + \Delta P_e^{-}(s) \cdot \lambda_{\Delta e}^{-} \tag{7}$$

$$\Delta P_r(s) \cdot \lambda_{\Delta r} = \Delta P_r^{+}(s) \cdot \lambda_{\Delta r}^{+} + \Delta P_r^{-}(s) \cdot \lambda_{\Delta r}^{-} \tag{8}$$

$$P_r^{\mathrm{sch}} = 200\mathrm{mHz} \cdot K \ \ (K \text{ is droop constant}) \tag{9}$$

$$P_r(s) = \Delta f \cdot K \ \ ; \ \ \Delta f = f_e - f_{\mathrm{ref}} \ (f_{\mathrm{ref}} \text{ is 50 Hz}) \tag{10}$$

where $P_r(s)$ and $P_e(s)$ are stochastic parameters, λ_e^{sch} and λ_r^{sch} are the electricity and reserve prices respectively. $\mathbb{E}_S$ is the probability of scenario s. $\Delta {P_e}^{+}(s)$, $\Delta {P_e}^{-}(s)$, $\Delta {P_r}^{+}(s)$ and $\Delta {P_e}^{+}(s)$ are additional and deficiency of power injection to the grid and reserve provision. $\lambda_{\Delta e}^{-}$, $\lambda_{\Delta e}^{+}$, $\lambda_{\Delta r}^{-}$ and $\lambda_{\Delta r}^{+}$ are revenue and penalty for additional power and reserve injected to the grid as well. The optimization will be carried out for 24 hours, considering market parameters on a quarter-hourly basis. ΔT is the time interval for electricity injection and frequency regulation, i.e., 15 minutes. The TSO has different mechanisms to penalize providers if they violate their scheduled reserve contributions based on the contracted agreement. The imbalance in energy settlement takes place in real-time on a quarter-hourly basis. Consequently, the energy provider gets a reduced revenue and penalty for its positive

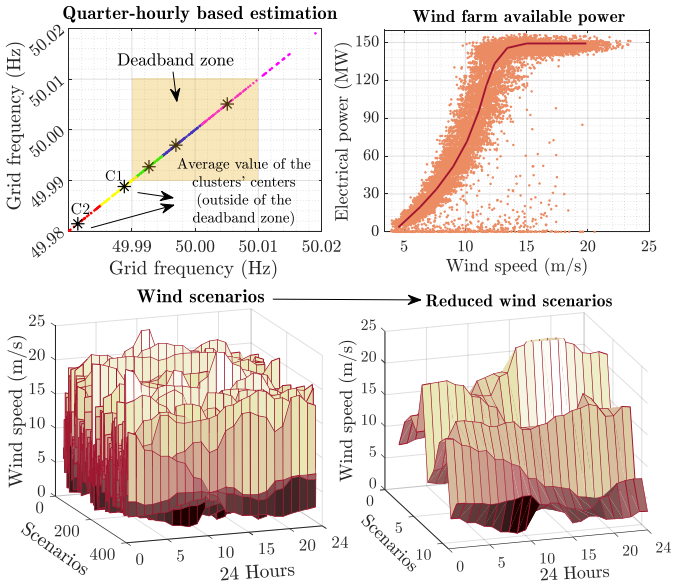

Figure 3: Stochastic parameters based on historical datasets.

and negative deviation at each settlement course when the generated power is higher than the scheduled power as follows:

$$\lambda^{+}_{\Delta e} = \lambda^{\text{sch}}_{e} - \alpha \quad ; \quad \lambda^{-}_{\Delta e} = \lambda^{\text{sch}}_{e} + \alpha \tag{11}$$

$$\lambda^{-}_{\Delta r} = 0.2 \cdot \Theta \cdot \lambda^{\text{M}}_{r} \quad ; \quad \lambda^{+}_{\Delta r} = 0 \tag{12}$$

$$\Theta = \frac{P^{\text{sch}}_{r} - P_{r}}{P^{\text{sch}}_{r}} \tag{13}$$

where α is an additional incentive component, which depends on the average of the absolute values of the System Imbalance (SI) of the current and the previous imbalance settlement period [36]. Θ is the failure factor, which increases by the difference between the scheduled FCR and the activated one, i.e., P_r. λ^{M}_{r} is the total remuneration for the FCR awarded for month M [37]. The objective function (4) is subject to the following boundary conditions:

First stage:

$$0 \leqslant P^{\text{sch}}_{e} \leqslant P^{\max}_{\text{wf}} \quad ; \quad 0 \leqslant P^{\text{sch}}_{r} \leqslant \frac{P^{\text{sch}}_{e}}{2} \tag{14}$$

$$P^{\text{sch}}_{e} + P^{\text{sch}}_{r} \leqslant P^{\max}_{\text{wf}} \tag{15}$$

Second stage:

$$0 \leqslant P_{e}(s) \leqslant P^{\text{av}}_{\text{wf}} \quad ; \quad 0 \leqslant P_{r}(s) \leqslant \frac{P_{\text{r}}(s)}{2} \tag{16}$$

$$\Delta P^{+}_{e}(s) = P_{e}(s) - P^{\text{sch}}_{e} \quad \text{if} \quad P_{e}(s) > P^{\text{sch}}_{e} \tag{17}$$

$$\Delta P^{+}_{r}(s) = P_{r}(s) - P^{\text{sch}}_{r} \cdot \Delta f \quad \text{if} \quad P_{r}(s) > P^{\text{sch}}_{r} \tag{18}$$

$$\Delta P^{-}_{e}(s) = P_{e}(s) - P^{\text{sch}}_{e} \quad \text{if} \quad P_{e}(s) \leqslant P^{\text{sch}}_{e} \tag{19}$$

$$\Delta P^{-}_{r}(s) = P_{r}(s) - P^{\text{sch}}_{r} \cdot \Delta f \quad \text{if} \quad P_{r}(s) \leqslant P^{\text{sch}}_{r} \tag{20}$$

where the piece-wise linearization of the P_{wf} given in (3) is used to find the optimal solutions. The constraints (14) and (15) limit the scheduled electricity and reserve contribution to the WF's maximum capacity. The constraints (16) restrict the electricity and reserve activation to the available WF output power. The half capacities in (14) and (16) guarantee the upward and downward regulations when the grid frequency drops or goes above 50 Hz, considering the deadband zone. The constraints in (16) are the limitations for electricity injection and reserve activation. The constraints (17) to (20) are considered for penalizing the electricity extra injection/off-takes and over/under reserve activations against the schedule.

IV. Optimal Operation Strategy

A. Wind farm operation

When the total available power $P^{\text{av}}_{\text{wf}}$ is higher than the scheduled power reserve P^{sch}_{r}, the WF is able to deliver FCR in response to the grid frequency variations. The extra power that should be arranged among N WTs can be referred to as the WF deloaded power:

$$P^{\text{dl}}_{\text{wf}} = P^{\text{av}}_{\text{wf}} - P^{\text{sch}}_{r} \quad ; \quad P^{\text{av}}_{\text{wf}} = \sum_{i=1}^{N} P_{w,i}(v_i) \tag{21}$$

and v_i is the wind speed experienced by each turbine. The electrical power of each WT and the rotor thrust can be expressed as:

$$P_{w,i} = \frac{1}{2}\rho R^2 v_i^3 C_p(\lambda_i, \theta_i) \tag{22}$$

$$F_{w,i} = \frac{1}{2}\rho R^2 v_i^2 C_T(\lambda_i, \theta_i) \tag{23}$$

where ρ is the air density and R is the blade length. $C_P(\lambda_i, \theta_i)$ and $C_T(\lambda_i, \theta_i)$ are the power and thrust coefficients that vary with the individual tip speed ratio $\lambda_i = R\omega_i/v_i$ and blade pitch angle θ_i. An empirical $C_p(\lambda, \theta)$ equation can also be found in literature [38], with an exponential form as follows:

$$C_P(\lambda, \theta) = c_1 \left(\frac{c_2}{\lambda_J} - c_3\theta - c_4 \right) e^{\frac{-c_5}{\lambda_J}} \tag{24}$$

$$\frac{1}{\lambda_J} = \frac{1}{\lambda + c_6} - \frac{c_7}{\theta^3 + 1} \tag{25}$$

where coefficients $c_1, ..., c_6$ for MW size WTs are 0.22, 116, 0.4, 5, 12.5, 0.088, and 0.035 respectively [39]. The thrust coefficient is modeled by a second-order polynomial function obtained from a wide range of simulations carried out using the NREL 5-MW offshore baseline WT:

$$C_T(\lambda, \theta) = \varepsilon_1 + \varepsilon_2\theta + \varepsilon_3\lambda + \varepsilon_4\theta^2 + \varepsilon_5\theta\lambda + \varepsilon_6\lambda^2 \tag{26}$$

where $\varepsilon_1, ..., \varepsilon_6$ are -0.1854, 0.0308, 0.161, 0.0002, -0.0133, and -0.0054, respectively. These results are derived for the robust fitness to the Least Absolute Residuals (LAR) with 0.9985 R-square and 0.067 RMSE.

B. Estimating wake formation

The conventional WF control approach relies on the WTs operating in Maximum Power Point Tracking (MPPT) mode without considering wake minimization strategies. However, in this study, two major optimal control approaches are considered, i.e., Axial Induction Control (AIC) and Wake Redirection Control (WRC). The AIC strategy reduces the upstream WTs' thrust force and controls wake formation by adjusting their axial induction factor by offsetting the blade pitch angle or tip speed ratio. The WRC strategy aims to steer the wakes away from downstream WTs by operating the WTs

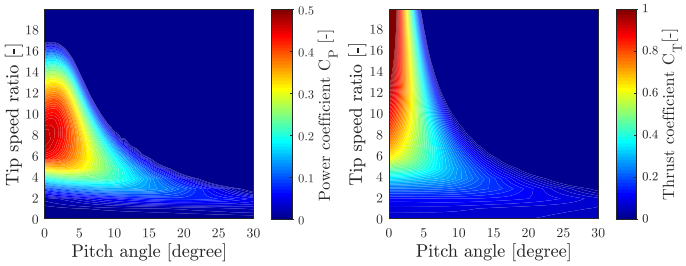

Figure 4: 5-MW WT Power and thrust coefficients.

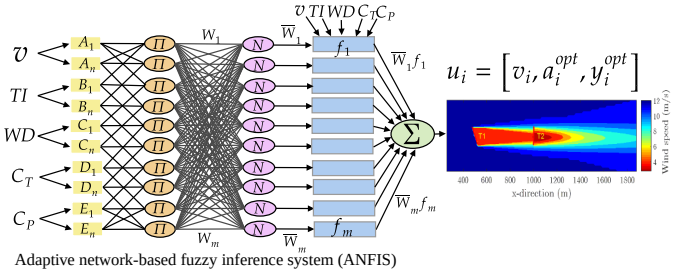

Figure 5: The ANFIS structure, estimating optimal wake parameters under AIC and WRC strategies.

with a yaw misalignment [40]. To achieve axial induction-based control, the free-streamed WTs need to be operated outside their aerodynamic maximum by increasing the blade pitch angle or reducing the tip-speed ratio (operating at a suboptimal working point). This reduces the WT power P_w and the magnitude of the rotor's thrust force, which depends on the thrust coefficient. The power coefficient C_P and thrust coefficient C_T of the 5-MW offshore turbine as a function of the pitch angle and tip speed ratio are shown in Fig. 4. The power and thrust coefficients can also be expressed as functions of axial induction factor a_i and nacelle yaw angle y_i (yaw misalignment) as follows:

$$C_P = 4a_i(\cos y_i - a_i)^2 \tag{27}$$

$$C_T = 4a_i\sqrt{\sin^2 y_i + (\cos y_i - a_i)^2} \tag{28}$$

The derivation of (27) and (28) involves using the axial momentum and the Glauert theory, which are widely used in theoretical models for predicting WT performance [41], [42]. The energy extraction by the turbine blades causes a reduction in the wind velocity at the turbine rotor disk. The average wind velocity at the turbine can be calculated by the axial induction factor $a_i \in [0, 1/3]$. The maximum C_P is determined by taking the derivative of the power coefficient (27) with respect to a_i and setting it equal to zero $\frac{\partial C_P}{\partial a_i} = 0$. In accordance with the Betz limit, $C_{P,max} = 16/27$ is the maximum theoretically possible rotor power coefficient [43]. Therefore, the maximum C_P can be achieved when $a_i = 1/3$ and zero degrees yaw misalignment y_i. Accordingly, from (28), the thrust coefficient for an ideal WT fully aligned with the wind, i.e., $y_i = 0$, is equal to $4a_i(1 - a_i)$. C_T has a maximum of 1.0 when $a = 0.5$ and the downstream velocity is zero. At maximum power output $a = 1/3$, C_T has a value of $8/9$.

In order to identify optimal setpoints for WTs that provide FCR, it is crucial to rapidly report the WF's optimal aerodynamic couplings and wake information. To accomplish this, a deep learning approach has been proposed that can model the WF's flow fields and accurately approximate turbine wake information. The Gauss-Curl-Hybrid wake model available in the FlOw Redirection and Induction in Steady State (FLORIS) simulation software is employed, which combines the Gaussian wake model and the curl wake model to accurately predict the wind speed deficit and turbulence intensity in the wake of a WT. The model also considers the effects of ambient turbulence and the coupling between C_P and C_T to maximize power production while minimizing the wake effects with the following objective function:

$$\begin{aligned} \max_{y_i, a_i} \quad & \sum_{i=1}^{N} P_{w,i}(a_i, y_i, v, WD) \\ \text{s.t.} \quad & -50.0^\circ \leq y_i \leq 50.0^\circ \\ & 0.0 \leq a_i \leq 0.3333 \end{aligned} \tag{29}$$

Optimal yaw angles y_i^{opt} and axial induction a_i^{opt} factors are estimated under AIC and WRC strategies in different wind conditions. Furthermore, extensive simulations are carried out offline to train and test the ANFIS structure shown in Fig.5. After training the ANFIS model with the obtained dataset, it can accurately replicate and mimic the complex wake deficits of a W for a wide range of conditions, including wind speeds, turbulence intensities, WDs, and turbine performance parameters such as C_P and C_T. By using these inputs, the model is capable of approximating the waked control operation and predicting the optimal values of v_i, y_i^{opt}, and a_i^{opt} for individual turbines within the W. Using the ANFIS model to estimate wake parameters allows for the rapid optimization of W performance by finding the optimal setpoints for individual turbines to contribute to frequency control reserves. Although the contracted scheduled reserve cannot be changed and must be respected hourly, the optimal allocation of power reserve can be actively updated when the wind field and wake formation vary.

C. Deloading strategy

WFs can provide power reserve and frequency control response (FCR) above nominal wind speeds. However, at wind speeds below the rated value, it may be necessary to deload some WTs to meet the promised FCR provision in case the grid frequency drops and extra power needs to be injected into the grid. Fig.6 shows that the deloaded operation of a WT can be achieved by shifting the operating point to the left or right of the maximum power point [44], [45]. This process creates a reserve margin by varying the active power between P^{dl} and P^{MPPT}, achieved by changing the rotor speed between ω^{dl} and ω^{MPPT}. It is preferred to shift the operating point to the right to prevent a decrease in kinetic energy, which is beneficial for an inertial response, and restrict the wake deficit while activating FCR. An adaptive look-up table is included in the supplementary control loop, as shown in Fig. 1, for estimating the deloaded power reference P^{dl}, capture and reflect the time-varying characteristic of the proposed power

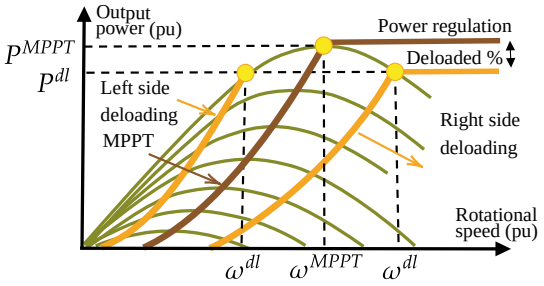

Figure 6: WT MPPT and deloaded power curves.

reserve, and to adjust the rotational speed dynamically. In this method, the reserve margin β represents the deloading percentage that specifies the upper limit of generated power and the saving margin that must be maintained as a constant power reserve. During low-frequency periods, utilizing the generation margin thus created, the WT active power can be controlled by varying the rotor speed between ω^{dl} and ω^{MPPT}. The pitch control system will also be activated to adjust the limitations of the axial induction factor a_i^{opt} to restrict the wake deficit. Moreover, the kinetic energy stored in rotating masses of WTs can also be released for the inertial response as further system support.

D. Optimization problem

The scheduled reserve capacity should be optimally distributed depending on the location of each turbine within a farm and the airflow deficits caused by upstream turbines operating with a higher rotational speed than MPPT. Therefore, optimal rotor speed estimation can be achieved by considering the conflict between maximum generated power, complex interactions among WTs, and maximizing kinetic energy, which can be formulated as follows:

$$E_{w,i} = \frac{1}{2} J_i \omega_i^2 \tag{30}$$

where J_i is the inertia of each turbine. The objective of the optimization problem is to maximize the total kinetic energy of the WF $E_{w,i}$ and the total output power of the WF $\sum P_{w,i}$. This can be achieved by operating some of the WTs in a sub-optimal operation mode, such that minimum wake deflection is produced. Consequently, the optimization problem for the optimal deloading control of WTs is given by:

$$\max_{\omega_i,\theta_i} \{f_1, f_2\} \qquad \omega_i, \theta_i \in \mathbb{R} \tag{31}$$

$$f_1 = \sum_{i=1}^{N} P_{w,i}(v_i, C_P(\omega_i, \theta_i)) \quad , \quad f_2 = \sum_{i=1}^{N} E_{w,i}(\omega_i) \tag{32}$$

s.t.

$$\underline{\omega_i} \leqslant \omega_i^{\mathrm{MPPT}} \leqslant \omega_i^{dl} \leqslant \overline{\omega_i} \tag{33}$$

$$\underline{\theta_i} \leqslant \theta_i^{\mathrm{offset}} \leqslant \overline{\theta_i} \tag{34}$$

$$C_{P_{w,i}}(\omega_i, \theta_i) \leqslant C_P(a_i^{\mathrm{opt}}, y_i^{\mathrm{opt}}) \tag{35}$$

$$C_{T_{w,i}}(\omega_i, \theta_i) \leqslant C_T(a_i^{\mathrm{opt}}, y_i^{\mathrm{opt}}) \tag{36}$$

$$\sum_{i=1}^{N} P_{w,i}^{\mathrm{dl}} = \sum_{i=1}^{N} P_{w,i}(v_i) - P_r^{\mathrm{sch}} \tag{37}$$

where $P_{w,i}$ and $E_{w,i}$ are given in (22) and (30) respectively. Constraints (33) and (34) limit the deloaded rotational speed and blade pitch angle offset to the allowable range. The maximum rotor speed is determined by the DC-link voltage of the power electronic converter, and the minimum rotor speed corresponds to the optimal tip speed ratio in MPPT mode. The constraints (35) and (36) ensure that the optimal power coefficient and thrust force of each WT are limited by the estimated optimal axial induction factors a_i^{opt} and yaw angles y_i^{opt} for the current wake formation given by the ANFIS model. These two constraints restrict the feasible space for searching the optimal rotor speed and blade pitch offset based on the unique wake formation caused by different scenarios of wind speed, direction, and TI. The constraint (37) also ensures maintaining the scheduled power reserve that has been foreseen for the WF to provide in the day-ahead market, which is discussed in (III). The optimal reserve allocation can be achieved by acting individually on pitch and torque control, ensuring sub-optimal operation for a given v_i, y_i^{opt} and a_i^{opt}, which are estimated by the method discussed in IV-B.

Algorithm 1 WT optimal power reserve allocation

Require: given historical datasets of gird frequency and wind speed, WF geometry, market clearance prices, system constraints, day-ahead forecasts, scenario selection.

Ensure:

for each hour τ of the operating day **do**

At the beginning of the τth hour:

Estimate quarter-hourly grid frequency fluctuations.

Use k-means clustering:

selecting the cluster centroids to represent Δf.

Find wind scenarios $s_1, \ldots, s_K$ from uncertainty set $\mathcal{S}$.

Estimating the expected value E_{s_K} of:

reduced set of scenarios for wind speed.

for $k = 1, \ldots, K$ **do**

Solve the second-stage problem:

$$z_k = \max g(P_e(s), P_r(s), \mathrm{E}_{s_K})$$

Solve the first-stage problem:

$$\max f(P_e^{\mathrm{sch}}, P_r^{\mathrm{sch}}) + \frac{1}{K} \sum_{k=1}^{K} z_k \quad \text{s.t.}(5-20)$$

Solve the MINLP problem using a suitable solver.

end for

submit the optimized bid P_r^{sch} for the 24-hour horizon.

During the whole hour:

for each τ' of the operating hour **do**

Measure v, TI, WD

Update the optimal wake parameters:

approximating $v_i, a_i^{\mathrm{opt}}, y_i^{\mathrm{opt}}$ using ANFIS model.

Solving (31) with constraints (33-37).

Return ω_i^{dl} and $\beta_i^{\mathrm{offset}}$

end for

end for

The proposed optimization problem aims to find the optimal rotational speed and blade pitch angle offset of the WTs to achieve the scheduled power reserve while actively updating

the optimal wake parameters for different wind scenarios during the operating hour. Algorithm 1 outlines the optimal power reserve allocation and deployment, taking into account the operation and wake constraints specified in (33-37). Since activating the power reserve will dynamically impact the wake parameters, the choice of shifting the operating point to the right side of the MPPT curve is made to not only increase kinetic energy for the inertial response but also restrict the wake parameters to stay within the predefined optimal ranges given in (35). At the same time, (36) ensures an optimal blade pitch offset that reduces the turbulence generated by the turbine and minimizes wake effects on downstream WTs while the WT activates FCR through the torque control system. This happens because of the unique nonlinear relationship between pitch and torque, which can only be fully controlled when the rotational speed exceeds the MPPT limit or when the wind speed goes above the rated value (the mentioned nonlinearities are visually illustrated in Fig.4). Therefore, although the pitch and torque control systems interact dynamically, wake formation will be actively controlled at the WT local control system by keeping the rotational speed variations in the right-side deloading zone (using an adaptive look-up table) while the blade pitch offset guarantees the optimal wake coordination when rotor speed changes due to the FCR activation in real-time.

It is worth mentioning that additional constraints and optimization objectives can be incorporated into the proposed problem formulation to further improve the system's performance. For instance, one can consider minimizing the cost of energy production by reducing mechanical loads and turbine wear and tear. This study mainly considered power production and kinetic energy, which mainly impact the WF's overall performance and wake mitigation. Moreover, different optimization algorithms can be explored to solve the problem efficiently, such as genetic algorithms, particle swarm optimization(PSO), or simulated annealing. This study considered multi-objective PSO to deal with the nonlinear optimization problem.

V. Case Study and Simulation Results

A. Optimal scheduled reserve

One of the most critical issues with the bidding strategies of WTs is the stochasticity of wind power and grid frequency. If the decision-maker offers a too-high bidding quantity, the operator will not be able to satisfy grid requirements at low wind speeds and will be subject to penalties. However, a low reserve bidding quantity leads to extra wind power curtailment and declines in revenue. The proposed optimization strategy compromises between an aggressive and a conservative decision with a high or low bidding quantity, considering the quarter-hourly based penalties and revenues defined by the TSO. Fig. 7 shows the estimated wind and grid frequency variations for a day in January 2020 and the calculated 24-hour optimal bidding schedule when the electricity and FCR prices are competitive (electricity and reserve were considered at the lowest and highest prices according to the energy market in 2019-2020). A windy day ($TI > 15\%$) is considered for studying different bidding scenarios. The proposed strategy

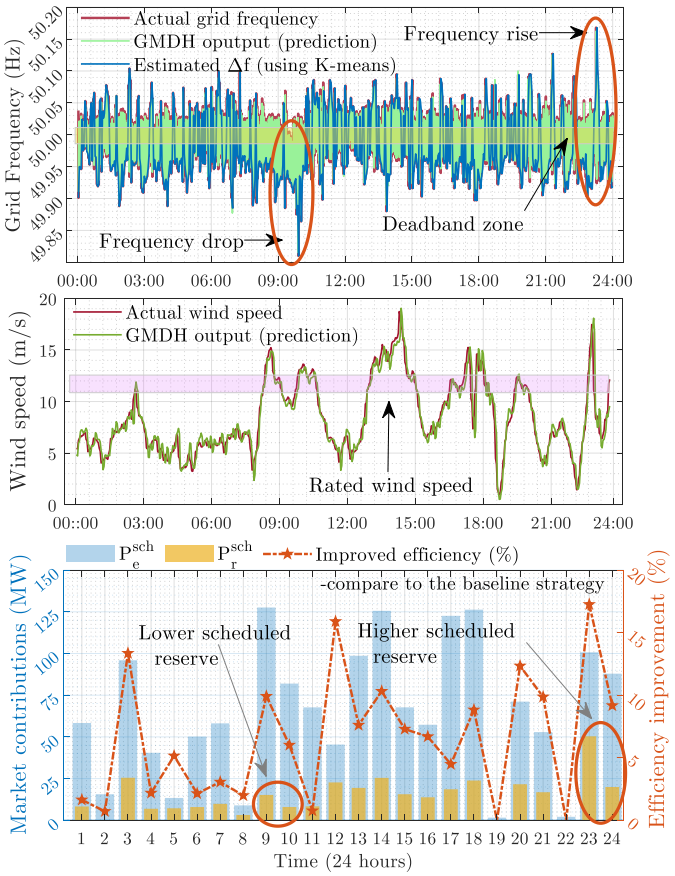

Figure 7: Estimated scheduled energy and reserve contribution. The time resolution of grid frequency and wind speed datasets is 10 seconds and 15 minutes, respectively.

is compared with the baseline approach, in which the WT contributes 10% of its capacity in the FCR market without considering the variability of wind and grid frequency, and the efficiency improvement is estimated, respectively. As Fig. 7 shows, higher contributions in both the energy and FCR are decided when the expected wind speed reaches the rated region. However, the lower or higher contribution in the day-ahead market is scheduled according to the estimation of maximum grid frequency deviation. For instance, although the wind speed goes above 11.4 m/s around 9:00-10:00h, a very low reserve bid is set due to the expected drop in grid frequency to avoid any penalty in case of a demanded upward regulation. In contrast, a higher contribution is set for reserve provision around 23:00-24:00h due to a rise in grid frequency considering the maximum possible downward regulation (reimbursing the curtailment by offering the FCR provision).

B. W wake modeling and optimal reserve allocation

This section evaluates the performance of the proposed optimal strategy for the 9.86 MW reserve provision that is decided around 7:00, where the mean wind speed is 7 m/s, and TI is 5%. Based on the results given in Fig.7, the optimal scheduled reserve around 7:00 clock is set to 9.86 MW when the average expected available wind power, considering different wake scenarios, is 38.13 MW. The studied wind

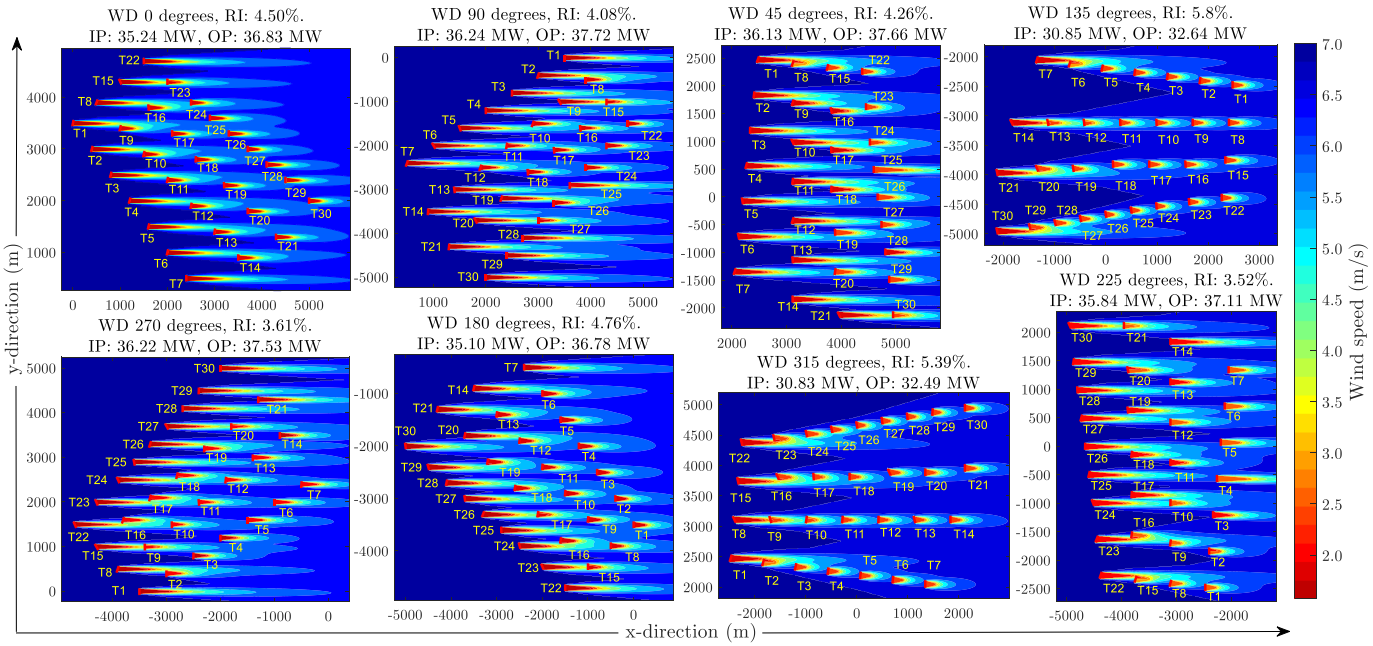

Figure 8: WF's wake modeling under the applied AIC and WRC strategies for 7 m/s wind speed and 5% turbulence intensity.

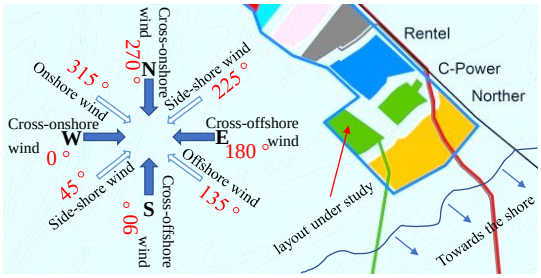

Figure 9: The WF layout in the North Sea.

directions WD are also illustrated in Fig.9, which addresses the geographic coordinates and indicates the onshore, offshore, side-shore, cross-offshore, and cross-onshore winds. Fig. 8 illustrates the WF modeling under the applied AIC and WRC strategies for the wind directions specified in Fig. 9, and power Relative Increase (RI) that percentiles the increase of Optimal Power (OP) based on the Initial Power (IP), where WTs greedily maximize their output power without considering negative impacts of the wake. The AIC approach involves adjusting the axial induction factor of each WT to mitigate the wake effects generated by upstream turbines. By optimizing the axial induction factor, AIC limits the excessive reduction in power output of downstream turbines, preventing significant loss due to wake effects. On the other hand, WRC adjusts the yaw angle of each WT to redirect the wake away from downstream turbines and reduce wake-induced power losses in the wind farm. As illustrated in Fig. 8, depending on the wind direction and the specific wake formation, the optimal wake parameters, i.e., yaw angles and axial induction factors, can be very different for various scenarios of wind direction. Therefore, The optimization problem (31) should be rapidly updated to find the optimal distribution of the power reserve in a varying wind condition. The computationally efficient estimation of WFs' optimal wake parameters, discussed in

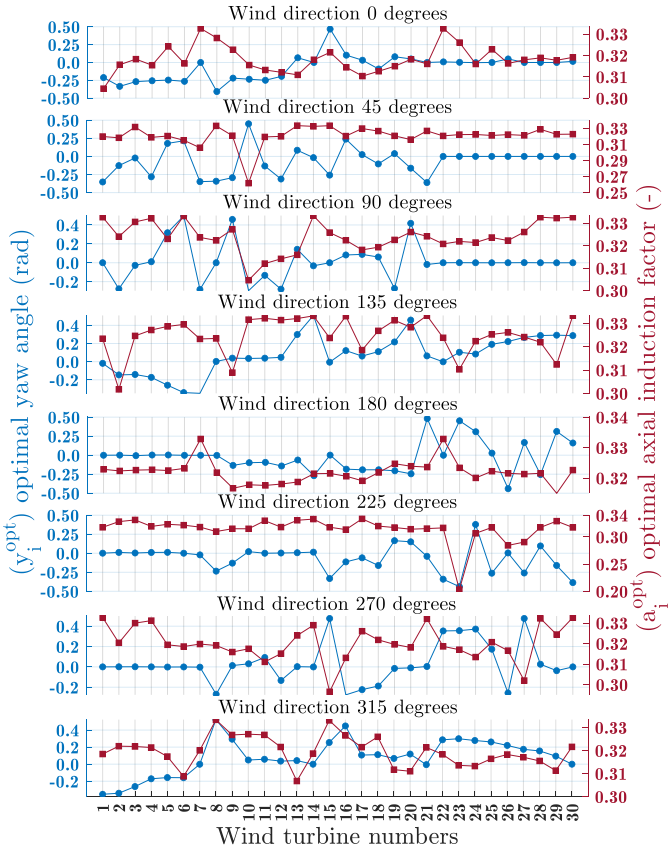

Figure 10: Estimated optimal wake parameters.

IV-B, are given in Fig.10, corresponding to the WF wake modeling under AIC and WRD strategies. The obtained wake information and optimal scheduled reserve can be fed into the optimization problem (31) to search for the optimal solutions, i.e., optimal deloaded rotor speeds and blade pitch angles (pitch offsets), maximizing the total power production and the

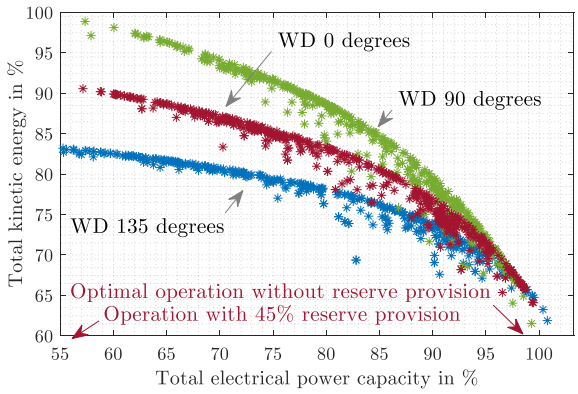

Figure 11: The Pareto front of the optimal solutions over the iterations of the bi-objective optimization problem.

kinetic energy. A co-evolutionary multi-swarm particle swarm optimizer based on crowding distance archival management is applied to find solutions in rapidly changing environments (the implementation of the proposed algorithm is given in the appendix). Fig. 11 illustrates the optimal solutions and Pareto fronts for the cross-offshore, cross-onshore, and offshore wind, which have the maximum, medium, and minimum kinetic capacity, respectively. It also shows that the maximum power production without any FCR provision should ensure 60% of the maximum total kinetic energy that can be released in inertial support. Also, the maximum total kinetic energy can only be achieved in the cross-offshore and cross-onshore wind by 45% deloading WTs (increasing the WTs' rotational speeds up to 45%). It can be comprehended that yawing upstream WTs control wake deflections. Also, the upstream WTs' axial induction factors are set to a lower value compared to the other WTs, which are less located in each other's stream with minimum wake overlaps. For instance, the axial induction factor of the upstream T1 (with maximum wake overlap) is set to 0.305 in the cross-onshore wind (WD0°). However, since T7 and T22 are almost decoupled from the WF wake, they are allowed to operate at their maximum capacity. The estimated power reserve is optimally distributed among the WTs by shifting their rotational speeds to the right side of the MPPT curve shown in Fig.6.

Moreover, the algorithm searches for the optimal individual blade pitch offset to ensure that the estimated WTs' optimal axial induction factors are respected. The total WF output should be deloaded by 19.86%. The Pareto front determines the maximum kinetic energy in different wind directions, the optimal deloaded rotational speeds, and the blade pitch offsets for the WTs. Fig.12 shows the power reserve allocation and presents the percentual share of each WT, identifying the WTs' deloading portion. For instance, T7 and T22 have the maximum share of FCR provision in the cross-onshore wind (WD0°) because they almost have no conflict with their neighboring WTs. Therefore, increasing their rotational speed will not cause wake disruption for their neighbors, and for the same reason, no blade pitch offset is required. However, as Fig.8 also visually confirms, T1 in the same wind direction can cause a significant wake for T9. Therefore, it plays a minimum contribution to FCR provision, and its operation

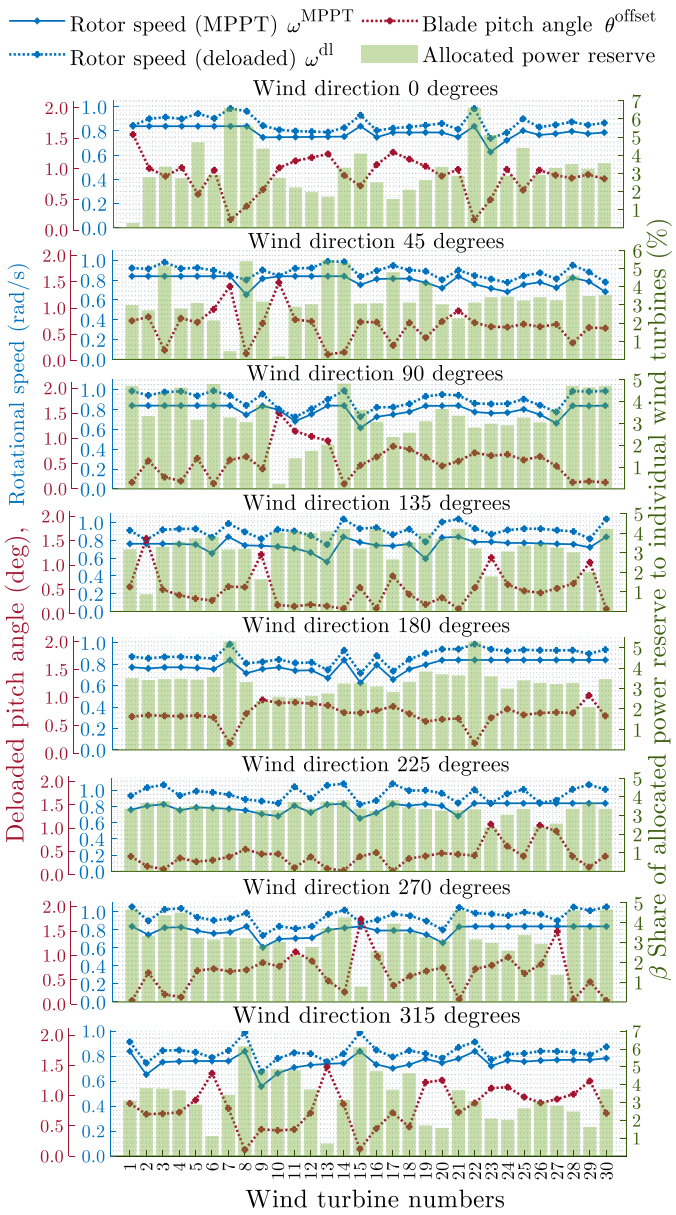

Figure 12: Optimal power reserve allocation for 7 m/s 5% TI wind speed, and 9.86 MW scheduled reserve.

will be limited by the optimal axial induction factor, which is achieved by a blade pitch offset of 1.6°. Taking advantage of the superior computational efficiency of the PSO and the proposed ANFIS model, the optimal power reserve allocation can be instantly updated by any changes in the dominant wind speed, direction, or TI. The performance of the proposed strategy is estimated and compared with the baseline strategy, where 15% reserve power is distributed evenly regardless of wake interactions. Furthermore, the simulations are carried out with different wind speeds and TIs concerning the dominant inflow wind direction [46] given in Fig.13. The results confirm the overall improvement and higher effectiveness at lower TIs, which cause stronger uniform wake formations and can play a significant role in the optimal allocation of power reserve.

Moreover, the dynamic behavior of the WF and the activation of the scheduled symmetric reserve have been in-

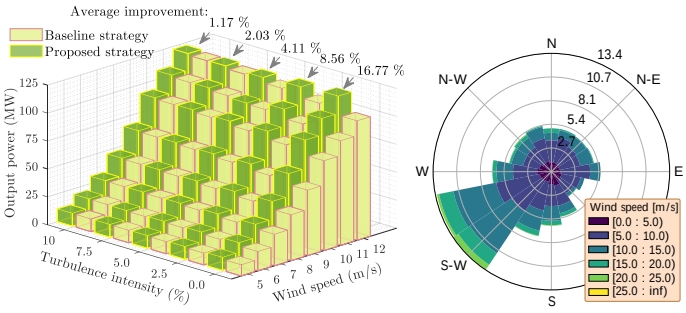

Figure 13: Performance of the proposed strategy for the S-W (side-shore) wind and wind rose for the C-Power layout.

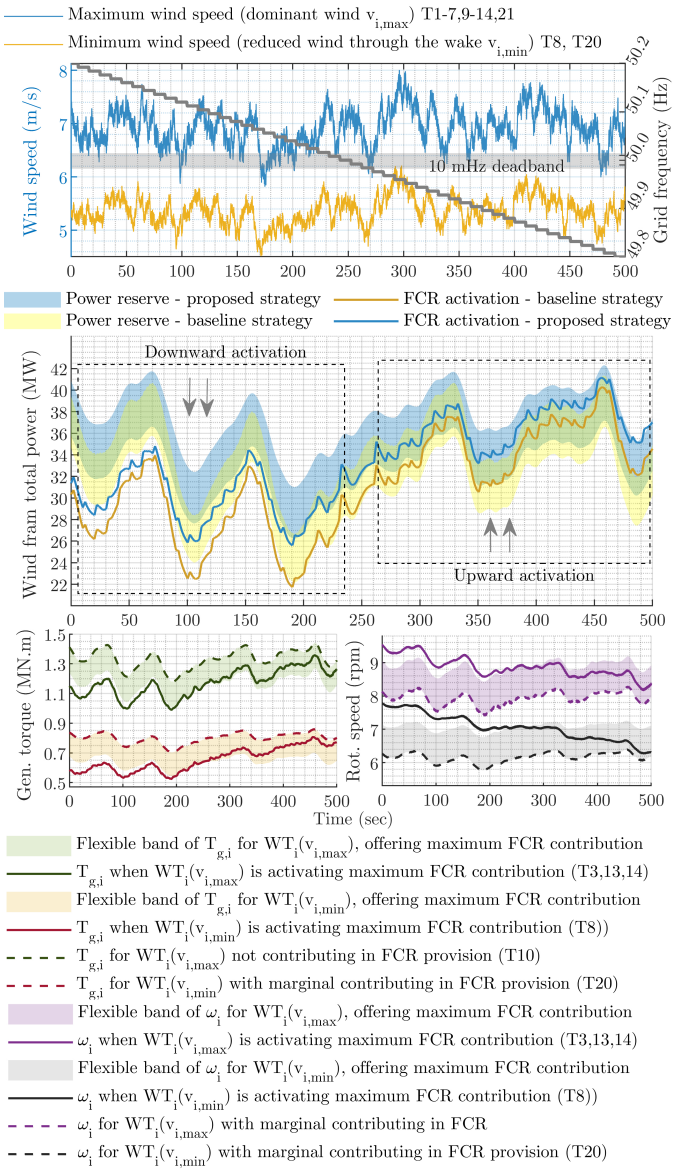

Figure 14: Dynamic operation of WF, activating 9.86 MW symmetric FCR for side-shore wind from the southwest.

vestigated based on the carried-out wake analysis. Fig. 14 depicts the active operation of the WF, which provides 9.86 MW symmetric FCR under turbulent wind conditions. The frequency profile utilized in this study is designed to simulate the worst-case scenario and is not representative of natural grid frequency behavior. This profile includes a significant drop from 50.2 to 49.8 Hz over 500 seconds to ensure the system can adequately respond to both upward and downward regulation during extreme conditions. The study examines the results of the dominant wind speed profile (maximum wind speed experienced by T1-7, T9-14, and T21) for the side-shore wind coming from the southwest with 7 m/s mean and 5% turbulence intensity (TI). T8 and T20 experience a minimum wind speed of 5.46 m/s through the wake deficit. The rest of the WTs receive reduced wind speeds between 7 and 5.46 m/s.

The WF's total power production has been estimated using the baseline control strategy that distributes the power reserve equally among WTs and the proposed optimal method that actively controls the wake and optimally allocates the scheduled reserve to WTs. As Fig. 14 visually depicts, although the efficiency improvement of the proposed strategy is practically greater than the baseline method, it can be noticed that it is more significant when the wind speed drops below the mean value. This is the direct effect of the active wake-controlled approach, which reduces the adverse impact of wakes and ensures the efficiency of the WTs at lower wind speeds. The deployment of the FCR, besides adjusting the blade pitch offset, yaw angle, and axial induction factor, dynamically involves regulating the WT's rotational speed and generator torque. Although FCR activation generally can be carried out through both pitch and torque control systems, in this study, to avoid introducing excessive mechanical loads on the WTs' blade's root and the tower, the FCR activation is done solely by adjusting the generator torque, and the pitch blade offset only keeps the WT operation in the acceptable optimal wake condition. These control actions and rotational speed variation between MPPT and deloaded operation (flexible band of ω_i) are also shown in Fig.14 for the maximum and minimum wind speeds with full and marginal FCR activations in different reserve allocations.

The optimization algorithm proposed in this study typically assigns a lower reserve to WTs located in the wake. Nevertheless, if the optimal yaw angle sufficiently redirects the wake and preserves wind speed, these turbines may also contribute to FCR provision. For instance, T8 receives a reduced mean wind speed of 5.44 m/s. However, with 50°yaw misalignment, its wake is redirected, and therefore, increasing its rotational speed up to 5% does not significantly reduce wind speed for T15 in its downstream path. Nevertheless, T20 is marginally involved in FCR contribution ($\beta < 3$) since its optimal yaw angle is decided for 25°, and its rotor speed increment can cause a significant wake for T29 and T28. Since wind direction changes can be frequent in the North Sea and alters the wake behavior, the proposed operation strategy suggests updating the power reserve allocation on a minutes scale (60 seconds $<$ tau' $<$ 600 seconds) to allow the WTs to optimize their power output in response to wind changing conditions and sub-hourly reserve schedules planned in the day-ahead market.

VI. Conclusions

This study proposes an operating strategy for WFs with optimal distribution of FCR. The studied algorithm supports optimal decision-making in the day-ahead market using the two-stage stochastic programming method considering data-driven wind speed forecasting and grid frequency for determining an hourly-based optimal scheduled reserve. Moreover, an optimization problem is formulated to dynamically allocate the estimated scheduled reserve among the WTs by actively minimizing wake interactions and maximizing WT's total electrical power and kinetic energy. A deep learning approach is suggested for computationally efficient estimation of the WT wake behavior under axial induction and wake redirection control strategies. The trained ANFIS model can mimic the WT's aerodynamic complexity in varying wind speed/direction and turbulence intensity and provides the optimization problem with appropriate constraints. The WT's desired control set points at the supervisory level will be determined by searching for the WTs' optimal deloading percentage, rotational speed, and blade pitch offset, leading to a relative increase in total generated power. The C-Power WF layout is studied to explore the aerodynamic coupling behavior in different wind directions. The creation of wake forms can significantly change the optimal allocation of power reserve and share of each WT in providing FCR. Results suggest that the proposed optimal operational framework can optimize the WTs' overall performance, especially in less turbulent conditions, and benefit WF owners willing to contribute to the day-ahead market without relying on a perfect storage system.

Acknowledgment

This research is part of the Energy Transition Fund project BEOWIND, funded by the Belgian federal government.

References

[1] T. Muneer, E. Jadraque Gago, and S. Etxebarria Berrizbeitia, "Wind energy and solar pv developments in the eu," in *The Coming of Age of Solar and Wind Power*. Springer, 2022, pp. 139–177.

[2] X. Yuan, C.-W. Su, M. Umar, X. Shao, and O.-R. LOBONŢ, "The race to zero emissions: Can renewable energy be the path to carbon neutrality?" *Journal of Environmental Management*, vol. 308, p. 114648, 2022.

[3] ESO. Technical report on the events of 9 august 2019. [Online]. Available: https://www.nationalgrideso.com/document/152346/download

[4] D.-Y. Li, P. Li, W.-C. Cai, Y.-D. Song, and H.-J. Chen, "Adaptive fault-tolerant control of wind turbines with guaranteed transient performance considering active power control of wind farms," *IEEE Transactions on Industrial Electronics*, vol. 65, no. 4, pp. 3275–3285, 2017.

[5] C. Edmunds, S. Martín-Martínez, J. Browell, E. Gómez-Lázaro, and S. Galloway, "On the participation of wind energy in response and reserve markets in great britain and spain," *Renewable and Sustainable Energy Reviews*, vol. 115, p. 109360, 2019.

[6] H. Wiklund, "The potential of wind power on the swedish ancillary service markets," 2021.

[7] ELIA, "Study on the future design of the ancillary service of voltage and reactive power control," 2018.

[8] K. Li, H. Guo, X. Fang, S. Liu, F. Teng, and Q. Chen, "Market mechanism design of inertia and primary frequency response with consideration of energy market," *IEEE Transactions on Power Systems*, 2022.

[9] H. Li, Y. Qiao, Z. Lu, B. Zhang, and F. Teng, "Frequency-constrained stochastic planning towards a high renewable target considering frequency response support from wind power," *IEEE Transactions on Power Systems*, vol. 36, no. 5, pp. 4632–4644, 2021.

[10] Y. Ma, Z. Hu, and Y. Song, "Hour-ahead optimization strategy for shared energy storage of renewable energy power stations to provide frequency regulation service," *IEEE Transactions on Sustainable Energy*, vol. 13, no. 4, pp. 2331–2342, 2022.

[11] S. Zhu, H. Wang, W. Wang, and X. Chang, "A combined day-ahead and intraday optimal scheduling strategy considering the joint frequency regulation reserve scheme among wind, photovoltaic and thermal power," *Frontiers in Energy Research*, vol. 10, p. 1965, 2023.

[12] A. E. Samani, N. Kayedpour, F. Kayedpour, J. D. De Kooning, G. Crevecoeur, and L. Vandevelde, "An optimal operation strategy for collaborative flexibility provision of a carbon capture and utilization process with wind energy," *IEEE Transactions on Sustainable Energy*, 2023.

[13] S. A. Hosseini, J.-F. Toubeau, Z. De Greve, and F. Vallée, "An advanced day-ahead bidding strategy for wind power producers considering confidence level on the real-time reserve provision," *Applied Energy*, vol. 280, p. 115973, 2020.

[14] Z. Zhang and Z. Chen, "Optimal wind energy bidding strategies in real-time electricity market with multi-energy sources," *IET Renewable Power Generation*, vol. 13, no. 13, pp. 2383–2390, 2019.

[15] A. Žertek, G. Verbič, and M. Pantoš, "Optimised control approach for frequency-control contribution of variable speed wind turbines," *IET Renewable power generation*, vol. 6, no. 1, pp. 17–23, 2012.

[16] M. Hedayati-Mehdiabadi, P. Balasubramanian, K. W. Hedman, and J. Zhang, "Market implications of wind reserve margin," *IEEE Transactions on Power Systems*, vol. 33, no. 5, pp. 5161–5170, 2018.

[17] M. Hedayati-Mehdiabadi, K. W. Hedman, and J. Zhang, "Reserve policy optimization for scheduling wind energy and reserve," *IEEE Transactions on Power Systems*, vol. 33, no. 1, pp. 19–31, 2017.

[18] H. Xiao, X. Huang, Y. Huang, and Y. Liu, "Self-synchronizing control and frequency response of offshore wind farms connected to diode rectifier based hvdc system," *IEEE Transactions on Sustainable Energy*, vol. 13, no. 3, pp. 1681–1692, 2022.

[19] C. Huang and H. Zhao, "Error-based active disturbance rejection control for wind turbine output power regulation," *IEEE Transactions on Sustainable Energy*, 2023.

[20] S. Boersma, B. Doekemeijer, S. Siniscalchi-Minna, and J. van Wingerden, "A constrained wind farm controller providing secondary frequency regulation: An les study," *Renewable energy*, vol. 134, pp. 639–652, 2019.

[21] A. K. Bhyri, N. Senroy, and T. K. Saha, "Enhancing the grid support from dfig-based wind farms during voltage events," *IEEE Transactions on Power Systems*, 2023.

[22] Z. Zhang, P. Kou, Y. Zhang, and D. Liang, "Coordinated predictive control of offshore dc collection grid and wind turbines for frequency response: A scheme without secondary frequency drop," *IEEE Transactions on Sustainable Energy*, 2023.

[23] M. De-Prada-Gil, C. G. Alías, O. Gomis-Bellmunt, and A. Sumper, "Maximum wind power plant generation by reducing the wake effect," *Energy conversion and management*, vol. 101, pp. 73–84, 2015.

[24] M. Dreidy, H. Mokhlis, and S. Mekhilef, "Inertia response and frequency control techniques for renewable energy sources: A review," *Renewable and Sustainable Energy Reviews*, vol. 69, pp. 144–155, 2017.

[25] A. Fernández-Guillamón, E. Gómez-Lázaro, E. Muljadi, and Ángel Molina-García, "Power systems with high renewable energy sources: A review of inertia and frequency control strategies over time," *Renewable and Sustainable Energy Reviews*, vol. 115, p. 109369, 2019.

[26] M. Kheshti, S. Lin, X. Zhao, L. Ding, M. Yin, and V. Terzija, "Gaussian distribution-based inertial control of wind turbine generators for fast frequency response in low inertia systems," *IEEE Transactions on Sustainable Energy*, 2022.

[27] J. Zhang, Y. Li, Z. Xu, D. Qi, and C. Li, "Game theory-based optimal deloading control of wind turbines under scalable structures of wind farm," *IET Cyber-Physical Systems: Theory & Applications*, vol. 3, no. 4, pp. 224–231, 2018.

[28] A. S. Ahmadyar and G. Verbič, "Coordinated operation strategy of wind farms for frequency control by exploring wake interaction," *IEEE Transactions on Sustainable Energy*, vol. 8, no. 1, pp. 230–238, 2016.

[29] S. Siniscalchi-Minna, F. D. Bianchi, M. De-Prada-Gil, and C. Ocampo-Martinez, "A wind farm control strategy for power reserve maximization," *Renewable energy*, vol. 131, pp. 37–44, 2019.

[30] Z. Zhang, M. Zhou, Z. Wu, S. Liu, Z. Guo, and G. Li, "A frequency security constrained scheduling approach considering wind farm providing frequency support and reserve," *IEEE Transactions on Sustainable Energy*, vol. 13, no. 2, pp. 1086–1100, 2022.

[31] X. Lyu, Y. Jia, and Z. Xu, "A novel control strategy for wind farm active power regulation considering wake interaction," *IEEE Transactions on Sustainable Energy*, vol. 11, pp. 618–628, 2020.
[32] ELIA. Transparency on grid data. [Online]. Available: https://www.elia.be/en/grid-data
[33] W. API. Sub-hourly historical weather. [Online]. Available: https://www.weatherbit.io/api/historical-weather-subhourly
[34] K. C. Sharma, P. Jain, and R. Bhakar, "Wind power scenario generation and reduction in stochastic programming framework," *Electric Power Components and Systems*, vol. 41, no. 3, pp. 271–285, 2013.
[35] N. Kayedpour, A. E. Samani, J. D. De Kooning, L. Vandevelde, and G. Crevecoeur, "A data-driven approach using deep learning time series prediction for forecasting power system variables," in *2019 IEEE 2nd International Conference on Renewable Energy and Power Engineering (REPE)*. IEEE, 2019, pp. 43–47.
[36] Elia. Day-ahead balance obligation of the balance responsible parties. [Online]. Available: https://www.elia.be/en/public-consultation/20200922-public-consultation-on-day-ahead-balance-obligation-of-brps
[37] Elia. Terms and conditions for balancing service providers for frequency containment reserve (FCR). [Online]. Available: https://www.elia.be/en/electricity-market-and-system/system-services/keeping-the-balance/fcrs
[38] J. D. M. De Kooning, L. Gevaert, J. Van de Vyver, T. L. Vandoorn, and L. Vandevelde, "Online estimation of the power coefficient versus tip-speed ratio curve of wind turbines," in *IECON 2013-39th Annual Conference of the IEEE Industrial Electronics Society*. IEEE, 2013, pp. 1792–1797.
[39] M. Carpintero-Renteria, D. Santos-Martin, A. Lent, and C. Ramos, "Wind turbine power coefficient models based on neural networks and polynomial fitting," *IET Renewable Power Generation*, vol. 14, no. 11, pp. 1841–1849, 2020.
[40] S. Boersma, B. M. Doekemeijer, P. M. Gebraad, P. A. Fleming, J. Annoni, A. K. Scholbrock, J. A. Frederik, and J.-W. van Wingerden, "A tutorial on control-oriented modeling and control of wind farms," in *2017 American control conference (ACC)*. IEEE, 2017, pp. 1–18.
[41] T. Burton, N. Jenkins, D. Sharpe, and E. Bossanyi, *Wind energy handbook*. John Wiley & Sons, 2011.
[42] K. S. Heck, H. M. Johlas, and M. F. Howland, "Modelling the induction, thrust and power of a yaw-misaligned actuator disk," *Journal of Fluid Mechanics*, vol. 959, p. A9, 2023.
[43] J. F. Manwell, J. G. McGowan, and A. L. Rogers, *Wind energy explained: theory, design and application*. John Wiley & Sons, 2010.
[44] K. Vidyanandan and N. Senroy, "Primary frequency regulation by deloaded wind turbines using variable droop," *IEEE transactions on Power Systems*, vol. 28, no. 2, pp. 837–846, 2012.
[45] X. Ge, X. Zhu, Y. Fu, Y. Xu, and L. Huang, "Optimization of reserve with different time scales for wind-thermal power optimal scheduling considering dynamic deloading of wind turbines," *IEEE Transactions on Sustainable Energy*, 2022.
[46] D. Allaerts, S. V. Broucke, N. van Lipzig, and J. Meyers, "Annual impact of wind-farm gravity waves on the belgian–dutch offshore wind-farm cluster," in *Journal of physics: conference series*, vol. 1037, no. 7. IOP Publishing, 2018, p. 072006.

APPENDIX

In this algorithm, each particle is evaluated for its fitness values with respect to two objective functions, f_1 and f_2. External archives $A_1, \ldots, A_K$ are used to store the non-dominated solutions encountered so far, and the best positions from these archives are used to update the particles in each iteration. The algorithm terminates after a maximum number of iterations T, and the final Pareto optimal set S and Pareto front F are generated by merging the external archives and selecting the non-dominated solutions, respectively. The function NonDominatedSort performs non-dominated sorting of the solutions in $A_k \cup P$ and returns the non-dominated solutions in A_k. After updating A_k, the algorithm checks if the size of A_k has exceeded the archive size K. If the size of A_k is greater than K, the crowding distance of solutions in A_k is calculated based on the f_1 and f_2 values. The solutions with the lowest crowding distance are then removed until the size of A_k is equal to K. This ensures that the external archive maintains a diverse set of non-dominated solutions by promoting well-spaced solutions in the objective space.

Algorithm 2 Co-evolutionary PSO with crowding distance archival management for bi-objective optimization

Require: Initial population of particles P, maximum number of iterations T, archive size K, fitness function $f_1(\cdot)$ and $f_2(\cdot)$
Ensure: Pareto optimal set S and Pareto front F
Initialize P and K external archives $A_1, \ldots, A_K$ with empty solutions
for $t = 1, \ldots, T$ **do**
  for $p \in P$ **do**
    Evaluate the fitness values of particle p:
    $f_1(p), f_2(p) \leftarrow f_1(p), f_2(p)$
    for $k = 1, \ldots, K$ **do**
      Update external archive A_k with the non-dominated solutions from the current population and the archive itself:
      $A_k \leftarrow \text{NonDominatedSort}(A_k \cup P)$
      if $|A_k| > K$ **then**
        Calculate crowding distance of solutions in A_k using the f_1 and f_2 values
        Remove solutions with the lowest crowding distance until $|A_k| = K$
      end if
    end for
  end for
  for $p \in P$ **do**
    Select a random external archive A_k
    Update particle p using the best position from A_k:
    $p.v \leftarrow w \cdot p.v + c_1 \cdot rand() \cdot (pbest - p) + c_2 \cdot rand() \cdot (best_{A_k} - p)$
    $p.x \leftarrow p.x + p.v$
  end for
end for
Generate the Pareto optimal set S by merging the solutions in the external archives $A_1, \ldots, A_K$:
$S \leftarrow A_1 \cup \cdots \cup A_K$
Generate the Pareto front F by selecting the non-dominated solutions from S:
$F \leftarrow p \in S : \nexists p' \in S^*$ such that:
$f_1(p') \leq f_1(p)$ and $f_2(p') \leq f_2(p)$

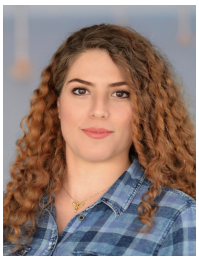

Nezmin Kayedpour (S'20) received a B.Sc. degree in electrical engineering and M.Sc. in Mechatronics, Robotics, and Automation Engineering from QIAU, Iran, in 2016. She is currently working towards a Ph.D. degree in electromechanical engineering in the Electrical Energy Laboratory, Department of Electromechanical, Systems and Metal Engineering at Ghent University, Belgium. Her current research interests include renewable energy applications, fuzzy logic, advanced optimization and data-driven control in smart grids, model-based fault diagnosis for dynamic processes employing artificial intelligence, and multi-criteria decision-making for the integration of wind farms. She is a member of the Flanders-Make@UGent MIRO core lab.

Arash E. Samani (S'20) received his B.S. degree in mechanical engineering from IAU University in Isfahan, Iran, in 2011 and his M.S. degree in mechanical engineering from Politecnico di Milano in Milan, Italy, in 2016. He completed his Ph.D. studies in electromechanical engineering at Ghent University in Belgium in 2022. He has conducted research in wind turbine performance analysis, aerodynamic modeling, and structural load analysis. He is currently engaged in research aimed at developing a novel approach to enhance the flexibility of power systems. His research seeks to facilitate the integration of renewables into power systems, thereby supporting the transition toward a low-carbon paradigm.

Farjam Kayedpour received a B.S. degree in Industrial Management from Raja University, Qazvin, Iran, in 2009, and subsequently pursued M.S. and Ph.D. degrees in production and operations management from the Allameh Tabataba'i University, Tehran, Iran, in 2012 and 2021 respectively. During his academic career, he conducted research on designing resilient supply chains and optimizing reliability models. Currently, his research interests include optimization modeling under uncertainty, fuzzy and robust optimization, evolutionary algorithms, reliability engineering, and supply chain management.

Jeroen D. M. De Kooning (M'09, SM'20) was born in Kapellen, Belgium, in 1987. He received the Bachelor, Master and Ph.D. degrees in electromechanical engineering from Ghent University, Belgium, in 2008, 2010 and 2015 respectively. Since 2019, he is assistant professor at the Department of Electromechanical, Systems and Metal Engineering at the Faculty of Engineering and Architecture of Ghent University, Belgium. In 2022, he was a visiting professor at the Lappeenranta University of Technology, Finland. He is a member of the Dynamical Systems and Control (DySC) research group and the Flanders-Make@UGent MIRO core lab. He conducted research on current waveform shaping techniques for permanent magnet synchronous machines, and optimal control and design of renewable energy systems. His present research interests include modelling, optimization and control of mechatronic systems, drivetrains and manufacturing machines in an Industry 4.0 context, with a particular interest in digital twins.

Lieven Vandevelde (M'05, SM'07) was born in Eeklo, Belgium in 1968. He graduated in electrical & mechanical engineering (main subject: electrical power engineering) at Ghent University in 1992 and is since then with the Electrical Energy Laboratory (EELAB), Department of Electromechanical, Systems and Metal Engineering, Ghent University. He received the Ph.D. degree from Ghent University in 1997, and has conducted research in various domains of electrical power engineering, *inter alia* electrical machines and (computational) electromagnetics. Since 2004, he has been member of the professorial staff and has been coordinating the research on electric power systems at EELAB. In this research, renewable energy and its integration in electric power systems play a prominent role.

Guillaume Crevecoeur Guillaume Crevecoeur (°1981) received his Master and PhD degree in Engineering Physics from Ghent University in 2004 and 2009, respectively. He received a Research Foundation Flanders postdoctoral fellowship in 2009 and was appointed Associate Professor at Ghent University in 2014. He is member of Flanders Make in which he leads the Ghent University activities on machines, intelligence, robotics and control. With his team, he conducts research on system identification and nonlinear control for mechatronics, industrial robotics and energy systems. His goal is to endow physical dynamic systems with improved functionalities and capabilities when interacting with uncertain environments, other systems and humans.